Symmetrization of 2D Vortices by Beat-Wave Damping

T. B. Mitchell* and C. F. Driscoll
Department of Physics and Institute for Pure and Applied Physical Sciences, University of California at San Diego, La Jolla, California 92093
(Received 28 March 1994)

Magnetized electron columns evolve in (r, θ) as 2D vortices in an incompressible inviscid fluid. Over a wide range of parameters, beat-wave resonance damping is observed to be the dominant vortex symmetrization mechanism. In this process, a (Kelvin or diocotron) surface wave decays to another surface wave of longer wavelength, with concomitant transport of vorticity.

PACS numbers: 47.32.Cc, 52.25.Wz, 52.35.Mw

Vortices are ubiquitous in energetic flows, and vortex dynamics strongly influence the energy transfers among long and short spatial scales. In 2D incompressible flow at high Reynolds numbers, merger and symmetrization of single-sign vorticity regions transfer energy to longer wavelengths, whereas filamentation and stretching generates mean-square vorticity and vorticity gradients on short spatial scales [1–3]. Here, we measure vortex symmetrization, and find that resonances, or "critical layers [4]," are crucial to understanding the decay of surface waves on an isolated, nominally circular vortex. These surface waves are called Kelvin waves in the fluids community [5] and diocotron waves in the plasma community [6–8].

For the historically useful idealization of a spatially constant 2D vorticity patch, one finds stable small amplitude Kelvin waves varying as $\sin(m\theta)$. The Kirchoff ellipse is an exact nonlinear solution [5] for $m = 2$, and nonlinear solutions for $m \geq 3$ have been found numerically and analytically [9]. However, this idealization precludes resonance between the wave and the fluid rotation at a radius where the vorticity is not spatially constant [10]. This "direct" resonance is now understood to give rise to inviscid spatial Landau damping of the wave [6]. For even moderate wave amplitudes, this damping is typically nonlinear, and the damping may either decrease [7] or cease [8] when the resulting "cat's-eye" flows generate fine-scale filaments inside (or partially outside [9,11]) the vortex. For "sharp-edged" vorticity profiles, the resonant radii can be completely outside the vortex, in which case no direct resonance damping occurs.

For general vorticity profiles, however, we find that a single-excited wave varying as $\sin(m\theta)$ will decay into a daughter wave varying as $\sin[(m-1)\theta]$, through "beat-wave" resonance damping of the nonlinear beat at frequency $\omega_m - \omega_{m-1}$ [12]. In this paper, we present observations of this decay instability and quantify the resulting exponential growth rates of the daughter waves. When the resonant coupling exists, a single Kelvin wave is an unstable equilibrium, and no equilibrium exists with two waves. This decay process is seen to give global symmetrization of an asymmetric vortex, while presumably also generating fine-scale resonance filaments within the vortex. For many vortex profiles, this beat-wave damping is observed to be the fastest mechanism for symmetrization.

The experimental apparatus [8,13,14] is shown in Fig. 1. A column of electrons is confined inside a series of conducting tubes of radius $R_w = 3.81$ cm and total length $L_w = 35$ cm, in a uniform axial magnetic field $B_z = 381$ Ga. The magnetic field provides radial confinement, and negative voltages applied to end tubes provide axial confinement. The rapid axial bounce motion of individual electrons effectively averages over any z variations, allowing a 2D description of the system.

The r, θ flow of the electrons is described by the 2D drift Poisson equations,

$$\frac{\partial n}{\partial t} + \mathbf{v} \cdot \nabla n = 0, \quad \mathbf{v} = -\frac{c}{B} \nabla \phi \times \hat{z}, \qquad \nabla^2 \phi = 4\pi e n, \tag{1}$$

where $n(r, \theta)$ is the (z-averaged) electron density, $\mathbf{v}(r, \theta)$ is the $\mathbf{E} \times \mathbf{B}$ drift velocity, and $\phi(r, \theta)$ is the electrostatic potential. The vorticity of the flow, $\zeta \equiv \hat{z} \cdot \nabla \times \mathbf{v} = n(4\pi ec/B)$, is proportional to the electron density, which is directly measured. These equations are isomorphic to the Euler equation [6,8]. A column of electrons in vacuum surrounded by a conductor thus evolves as would a 2D vortex in an incompressible inviscid fluid surrounded by a circular free-slip boundary.

In the experiments described here, an electron column is first injected and trapped, then azimuthally symmetrized using wall sectors to detect and damp any θ variations. A single mode with chosen azimuthal mode number m is then excited and allowed to evolve, while various

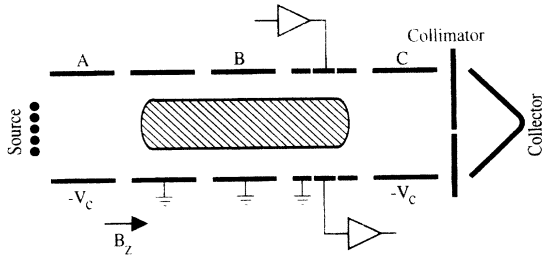

FIG. 1. Schematic of the cylindrical confinement geometry.

 0031-9007/94/73(16)/2196(4)$06.00

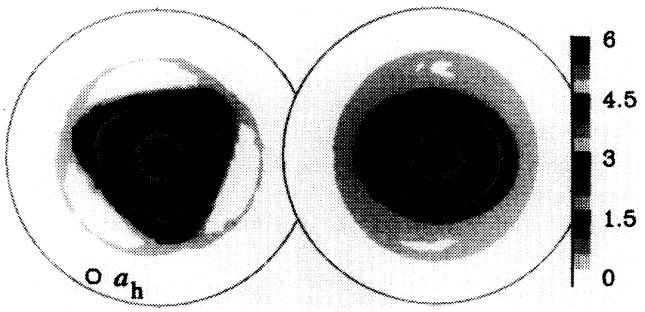

FIG. 2. Density (i.e., vorticity) contours showing an initial $m = 3$ excitation and the $m = 2$ wave plus diffuse halo, which evolves spontaneously in about 10 τ_R. Measurements are averaged over a collimator hole of area a_h.

mode amplitudes A_m are monitored with tuned filters. Finally, the electron column is dumped axially, and the charge which passes through a collimator hole of area $a_h = \pi(1.6 \text{ mm})^2$ at a particular r, θ position is measured. Wave growth and damping rates are obtained from a single evolution, but about 500 separate plasmas with identical initial conditions are required to generate a complete image of $n(r, \theta)$ [14].

We find that, in general, a single wave on a vortex will damp while causing exponential growth of waves with lower azimuthal mode number. Figure 2 shows the measured density (i.e., vorticity) distribution before and after beat-wave damping of an $m = 3$ perturbation on an otherwise symmetric column. This $m = 3$ parent mode decays rapidly to an $m = 2$ daughter mode plus a diffuse halo, on a time scale of 10 rotations of the vortex. The resultant $m = 2$ mode is then unstable to decay into an $m = 1$ mode. We note that the initial condition exhibits slight filamentation, due to direct resonance damping of the large $m = 3$ mode. This damping has saturated, since the resonant particles are all executing nonlinear orbits in the spatial cat's eye and is therefore incidental to the decay instability considered here.

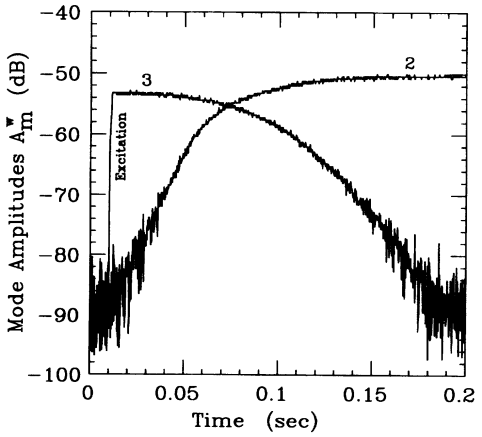

FIG. 3. Received wave amplitudes A_m^w vs time as an $m = 3$ wave decays to an $m = 2$ wave.

Figure 3 shows an example of the wave amplitudes A_m^w received from wall sectors during a $3 \rightarrow 2$ decay instability. For this evolution, the $m = 3$ wave was initially weak, with $A_3^w = -53$ dB, whereas the initial excitation of Fig. 2 was $A_3^w = -37$ dB. The $m = 2$ daughter mode grows exponentially with time until it becomes comparable in amplitude to the parent wave. Here, exponential growth is observed over 30 dB in daughter mode power (32× in amplitude), with a growth rate $\gamma_2 = 75 \text{ s}^{-1}$.

Figure 4 shows the measured amplitude growth rates of the daughter waves $\gamma_{m-1}\tau_R$ versus the normalized amplitudes of the parent wave A_m, for $m = 2$, 3, and 4. Here, the growth rates γ are scaled by the central rotation time $\tau_R \equiv 4\pi/\zeta(0) \equiv 2\pi/\omega_E(0) = 5.5$ μs. For comparison to theory, the mode amplitudes A_m are calculated from the θ components $\delta n_m(r)$ of the measured $n(r, \theta)$ by $A_m^2 \equiv \int d^2\mathbf{r}|\delta n_m(r)|^2 / \int d^2\mathbf{r}|n_0(r)|^2$. These measured density perturbations are directly proportional to the received wall signals, i.e., $A_m = g_m A_m^w$, with $g_2 = 3.5$, $g_3 = 7.8$, and $g_4 = 24$. These growth rates are all observed to depend on the vorticity profile; the profile for Figs. 3 and 4 is shown below in Fig. 5. Each data point is the average of three to five evolutions such as shown in Fig. 3, and the scatter in the measured rates is about the size of the symbols.

The $3 \rightarrow 2$ growth rate data are seen to scale as $\gamma_2 \propto A_3^2$ (shown by the dashed lines) over two decades in growth rate; for large A_3, the growth rates increase more rapidly. The $3 \rightarrow 2$ evolution of Fig. 3 corresponds to the Δ symbol at $A_3 = 1.7 \times 10^{-2}$, and the large amplitude excitation of Fig. 2 is similar to the Δ symbol at $A_3 = 0.11$.

A similar growth rate scaling is observed for the decay of an $m = 2$ wave into an $m = 1$ wave, shown as open circle symbols in Fig. 4. The data are close to $\gamma_1 \propto A_2^2$, again increasing more rapidly at the largest excitations. The largest $m = 2$ mode shown, with $A_2 = 0.44$, is an elliptical vortex with length/width aspect ratio $b/a = 1.6$. The smallest γ_1 growth rates have large error bars because the receiver electronics induces a damping $\gamma_1^e \approx$

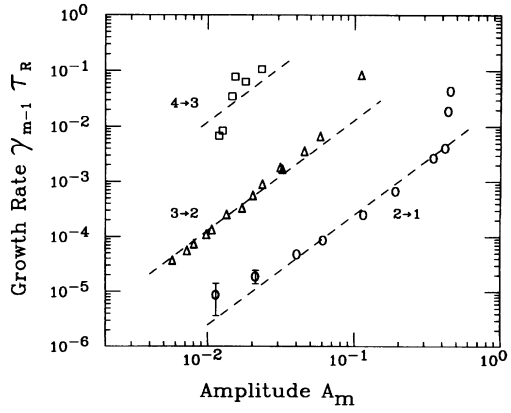

FIG. 4. Measured growth rates γ_{m-1} for daughter mode $m - 1$ (normalized to the vortex rotation time $\tau_R = 5.5$ μs) vs normed amplitude A_m of parent mode, for $m = 2$, 3, and 4. The dashed lines indicate $\gamma_{m-1} = \Gamma_{m,m-1}A_m^2$.

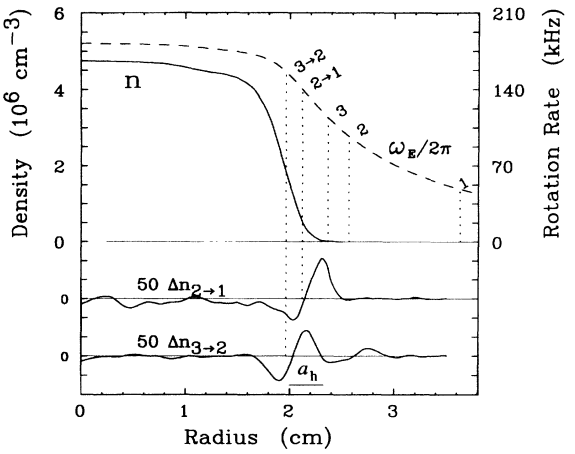

FIG. 5. Measured density profile $n(r)$; calculated fluid rotation $\omega_E(r)/2\pi$, with $m = 1, 2, 3$ direct resonance radii, and $2 \to 1$, $3 \to 2$ beat resonance radii; and measured perturbations $\Delta n(r)$ from $2 \to 1$ and $3 \to 2$ decay instabilities.

$-4.8\ s^{-1}$, and this rate has been subtracted from the data of Fig. 4. We note that the $m = 1$ mode exists only because our circular boundary breaks the translational symmetry of the system and that the characteristics of this one mode depend strongly on the wall position.

The same instability process is observed for $m = 4$ decaying to $m = 3$ (shown as squares in Fig. 4), although direct $m = 4$ resonance damping and low receiver sensitivity limit the range of data attainable. The largest $m = 4$ excitations here are quite weak, with diagonal/side ratios of about 1.04, yet the $m = 3$ mode e-folds in about nine vortex rotation times.

In general, the resonance damping results in an "inverse cascade" from high to low azimuthal mode numbers m, i.e., from shorter to longer wavelengths. To obtain the data for Figs. 2, 3, and 4, we often needed to limit this inverse cascade to one step by applying negative feedback at the $m - 2$ wave frequencies. In addition to the transfer to larger spatial scales, there is presumably transfer to short scales, due to the filamentary nature of the resonant damping; when spatially coarse grained, due to the collimator hole, this appears as a "halo" in Fig. 2.

Linear surface (Kelvin) waves on an isolated vortex with profile $n(r)$ are eigenfunctions $\delta n_m(r)$ and $\delta\phi_m(r)$ multiplying $\exp(im\theta - i\omega_m t)$. Linearizing Eqs. (1) then gives an eigenvalue equation [6] for ω_m,

$$\left(\frac{1}{r}\frac{\partial}{\partial r}r\frac{\partial}{\partial r} - \frac{m^2}{r^2}\right)\delta\phi_m = -\left(\frac{4\pi ecm}{rB}\right) \times \frac{\partial n/\partial r}{\omega_m - m\omega_E(r)}\delta\phi_m, \quad (2)$$

where the fluid rotation frequency is

$$\omega_E(r) \equiv \frac{c\partial\phi/\partial r}{rB} = \frac{2ce}{r^2B}\int 2\pi r'\,dr'\,n(r'). \quad (3)$$

For the theoretical construct of a circular constant vorticity "patch" of radius R_p surrounded by a wall at R_w, one obtains linear mode frequencies [15] $\omega_m = \omega_E[m - 1 + (R_p/R_w)^{2m}]$. In the absence of a wall, exact nonlinear solutions to Eqs. (1) can be obtained: An elliptical (Kirchoff) patch [5] with aspect ratio b/a rotates with frequency $\omega_2 = \omega_E 4ab/(a + b)^2$, and this has been generalized to higher m modes [9]. The vortex patch approximation predicts frequencies [8] and motions [16] reasonably close to those measured experimentally on vortices with monotonically decreasing profiles, although 3D axial confinement corrections may need to be included for both plasmas [14,17] and fluids [18].

A direct resonance between surface waves and the fluid flow occurs at a radius r_s, where $\omega_m = m\omega_E(r_s)$. When the vorticity profile is not constant near r_s, i.e., $\partial n/\partial r|_{r_s} \neq 0$, this resonance results in inviscid Landau damping [6] of the wave, with concomitant radial (and angular) transport of vorticity. This damping is represented schematically in Fig. 6(a). When this damping is present, the Kelvin wave is not strictly a normal mode of the system. Resonant damping of the wave results in spatial cat's eye [6,10] extending between flow x points separated by $\delta\theta = 2\pi/m$, with radial extent dependent on wave amplitude. Linear damping treats the case where the wave damps before a cat's-eye trapping oscillation occurs. Larger amplitude waves result in cat's-eye flows which when averaged over θ appear as radial transport from slightly inside to slightly outside the resonance [7]. For very large amplitude waves, this resonance may occur even when no resonance exists for the circular profile, and the cat's-eye flows appear as external filaments [8,11].

The decay instability observed here is apparently due to resonant damping of the beat wave resulting from nonlinear interaction of the pump and growing mode, shown schematically in Fig. 6(b). The nonlinear couplings involved in beat-mode damping have been treated theoretically by Crawford and O'Neil [12], although no quantitative coupling rates Γ_{ij} have yet been calculated. Energy and angular momentum conservation between waves and particles predicts that the coupling between pump mode i and daughter mode j will occur at a radius r_s, where

$$\omega_i - \omega_j = \omega_E(r_s^{i\to j})(i - j). \quad (4)$$

The unstable mode j is predicted to grow as

$$\frac{d}{dt}A_j = (-\gamma_j + \Gamma_{ij}A_i^2)A_j, \quad (5)$$

where γ_j is the linear damping of mode j and the coupling rate Γ_{ij} is independent of amplitude A_i for small A_i. A

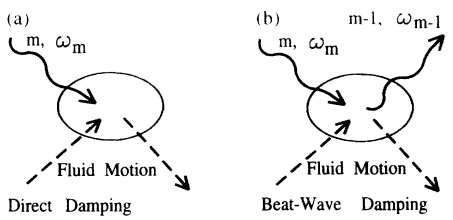

FIG. 6. Diagrammatic representation of (a) direct spatial Landau damping and (b) beat-wave damping.

similar nonlinear coupling to *external* field asymmetries A_i gives rise to an "induce scattering instability" which has been previously observed on these electron systems [19].

The predicted dependence on the square of the pump mode amplitude A_i in Eq. (5) agrees with the experimental data of Fig. 4. This allows us to estimate the coupling rates Γ_{ij}: The dashed lines in Fig. 4 give $\Gamma_{21} = 0.025/\tau_R$, $\Gamma_{32} = 1.3/\tau_R$, and $\Gamma_{43} = 120./\tau_R$. Also, it is observed experimentally that there is generally a threshold in mode amplitude below which no decay instability is observed. This presumably is due to the $-\gamma_j$ term, although this is sensitive to apparatus setup and has not been investigated quantitatively.

Most significantly, the beat-mode damping resonance signature of Eq. (4) is clearly seen in the measured perturbations in vorticity induced by the decay process. Figure 5 shows the measured z-averaged density profile $n(r)$ before any waves are excited, and the vortex rotation frequency $\omega_E(r)$ calculated from $n(r)$. The initial density profile was chosen so as to have no direct spatial resonances for modes $m \leq 3$, i.e., the measured mode frequencies projected onto $\omega_E(r)$ give resonant radii r_s at which there is essentially no vorticity. (For this profile, we measure $f_1 = \omega_1/2\pi = 48.4$, $f_2 = 188.3$, $f_3 = 344.2$, and $f_4 = 514.5$ kHz.) In contrast, the beat frequencies $\omega_2 - \omega_1$ and $\omega_3 - \omega_2$ have resonant radii $r_s^{2\to1}$ and $r_s^{3\to2}$ from Eq. (4) on the edge of the vorticity profile.

To obtain the vorticity perturbation induced by the decay instability, we subtract $n(r)$ from the profile measured after mode m is excited and decays to mode $m - 1$, and mode $m - 1$ is damped by applied feedback. To minimize systematic errors due to naturally occurring transport, $n(r)$ is actually measured after growing mode m, suppressing the growth of mode $m - 1$ and then damping mode m. Furthermore, the process is sequentially performed 10 times to obtain a measurable Δn from low-amplitude excitations. The measured $\Delta n_{2\to1}$ shows particles transported from immediately inside to immediately outside $r_s^{2\to1}$. The same signature is seen for $\Delta n_{3\to2}$, with an apparent error of 0.3 mm in the calculation of $r_s^{3\to2}$. The true structure of the perturbation is probably narrower than the features in Fig. 5, due to averaging over the collimator area a_h; also, the effects of fine-scale diffusion or viscosity [13] are not resolved.

In conclusion, we find that the relaxation of surface waves on an isolated magnetized electron column within a circular boundary is dominated by damping from beat wave resonances. Damping from direct resonances is also observed, but with a relatively sharp-edged vorticity profile, this damping saturates with the transport of all available resonant particles. Our observations show that surface wave damping from direct and beat-wave resonances should contribute significantly to the relaxation of vortices in inviscid 2D flows. Indeed, the beat-wave damping measured here suggests that, when there are available longer-wavelength modes, surface waves of finite amplitude will always be damped, and fine-scale filamentation or cat's eye within or outside the vortex will be generated. One consequence of this beat-wave damping is that a long-wavelength mode (such as an $m = 2$ ellipse) would appear to actively damp or suppress shorter wavelength modes such as $m = 3$. Finally, we note that these shape distortions are an inherent result of vortex-vortex interactions [16], including those leading to merger [20] or filamentation [21], so direct damping and beat-wave damping may affect these interaction processes.

This work was supported by Office of Naval Research Grant No. N00014-89-J-1714 and National Science of Foundation Grant No. NSF PHY87-06358. The authors acknowledge theory discussions with T. M. O'Neil, R. A. Smith, and W. G. Flynn.

*Present address: Los Alamos National Laboratory, K-480, Los Alamos, NM 87545.

[1] J. C. McWilliams, J. Fluid Mech. **146**, 21 (1984).
[2] R. Benzi, S. Patarnello, and P. Santangelo, Europhys. Lett. **3**, 811 (1987).
[3] G. F. Carnevale *et al.*, Phys. Rev. Lett. **66**, 2735 (1991).
[4] S. A. Maslowe, Annu. Rev. Fluid Mech. **18**, 405 (1986).
[5] H. Lamb, *Hydrodynamics* (Dover, New York, 1932) 6th ed., Secs. 158, 159.
[6] R. J. Briggs, J. D. Daugherty, and R. H. Levy, Phys. Fluids **13**, 421 (1970); R. H. Levy, Phys. Fluids **8**, 1288 (1965).
[7] J. S. deGrassie and J. H. Malmberg, Phys. Fluids **23**, 421 (1980); S. Pillai and R. W. Gould, Bull. Am. Phys. Soc. **38**, 1970 (1993).
[8] C. F. Driscoll and K. S. Fine, Phys. Fluids B **2**, 1359 (1990).
[9] D. I. Pullin, Annu. Rev. Fluid Mech. **24**, 89 (1992).
[10] W. Kelvin, Nature (London) **23**, 45 (1880).
[11] M. V. Melander, J. C. McWilliams, and N. J. Zabusky, J. Fluid Mech. **178**, 137 (1987).
[12] J. D. Crawford and T. M. O'Neil, Phys. Fluids **30**, 2076 (1987).
[13] C. F. Driscoll, J. H. Malmberg, and K. S. Fine, Phys. Rev. Lett. **60**, 1290 (1988).
[14] T. B. Mitchell, Ph.D. thesis, University of California at San Diego (1993).
[15] S. A. Prasad and T. M. O'Neil, Phys. Fluids **26**, 665 (1983).
[16] T. B. Mitchell, C. F. Driscoll, and K. S. Fine, Phys. Rev. Lett. **71**, 1371 (1993).
[17] A. J. Peurrung and J. Fajans, Phys. Fluids B **5**, 4295 (1993).
[18] G. F. Carnevale, P. Cavazza, and R. Purini, Phys. Fluids A **3**, 1411 (1991).
[19] D. L. Eggleston and J. H. Malmberg, Phys. Rev. Lett. **59**, 1675 (1987).
[20] K. S. Fine *et al.*, Phys. Rev. Lett. **67**, 588 (1991).
[21] D. G. Dritchell and D. W. Waugh, Phys. Fluids A **4**, 1737 (1992).

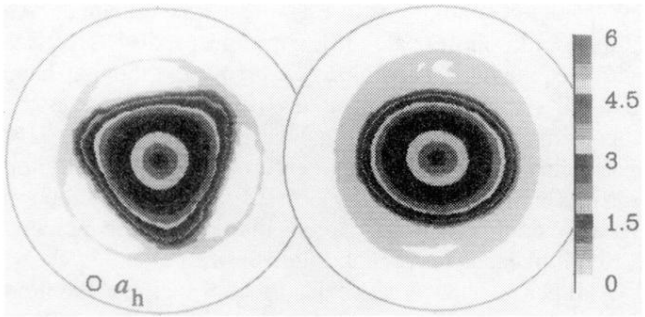

FIG. 2. Density (i.e., vorticity) contours showing an initial $m = 3$ excitation and the $m = 2$ wave plus diffuse halo, which evolves spontaneously in about 10 τ_R. Measurements are averaged over a collimator hole of area a_h.